European Polymer Journal 110 (2019) 283–292

Contents lists available at ScienceDirect

European Polymer Journal

journal homepage: www.elsevier.com/locate/europolj

DOX/ICG-carrying γ-PGA-g-PLGA-based polymeric nanoassemblies for acid-triggered rapid DOX release combined with NIR-activated photothermal effect

Kai-Ting Hou[a], Te-I Liu[a], Hsin-Cheng Chiu[a], Wen-Hsuan Chiang[b,*]

[a] Department of Biomedical Engineering and Environmental Sciences, National Tsing Hua University, Hsinchu 300, Taiwan
[b] Department of Chemical Engineering, National Chung Hsing University, Taichung 402, Taiwan

ARTICLE INFO

Keywords:
Amphiphilic graft copolymers
Polymeric nanoassemblies
Intracellular drug delivery
pH-triggered DOX release
NIR-activated photothermal treatment

ABSTRACT

To boost the efficacy of chemo-photothermal cancer treatment by the intracellular rapid release of doxorubicin (DOX) combined with near-infrared (NIR)-triggered photothermal effect of indocyanine green (ICG), the poly(γ-glutamic acid)-g-poly(lactic-co-glycolic acid) (γ-PGA-g-PLGA)-based polymeric nanoassemblies (PNAs) with simultaneous incorporation of DOX and ICG were developed in this work by simple one-step nanoprecipitation. The obtained DOX/ICG-loaded PNAs were characterized by a compact γ-PGA/DOX complexes-encapsulated PLGA-rich core covered with the co-assembly of amphiphilic D-α-tocopheryl polyethylene glycol succinate (TPGS), 1,2-distearoyl-sn-glycero-3-phosphoethanolamine-N-[amino(polyethylene glycol)] (DSPE-PEG) and ICG molecules. The robust cargo-loaded PNAs not only promoted the photo-stability of ICG in PBS, but also reduced ICG leakage from PNAs. With the milieu pH being altered from 7.4 to 5.0, the massive disruption of ionic DOX/γ-GA complexes and PLGA degradation considerably accelerated DOX release from payload-containing PNAs. The results of in vitro cellular uptake revealed that the DOX/ICG-loaded PNAs appreciably enhanced the cellular uptake of payloads by HeLa cells. Notably, through the intracellular acid-triggered rapid DOX release combined with the ICG-based NIR-activated hyperthermia and singlet oxygen generation, the combination therapy of DOX/ICG-loaded PNAs can use lower dosage of drugs to effectively inhibit proliferation of HeLa cells compared to the chemo or photothermal treatment alone, thus showing the great potential to improve efficacy of cancer treatment.

1. Introduction

In the past two decades, chemotherapy has been extensively utilized to treat a variety of cancers [1–4]. However, until now, cancer has been one of the most fatal illnesses around the world, thus revealing that only single chemotherapy to treat cancer remains inadequate. It has been recently reported that the combination of therapeutic modalities with multiple drugs and mechanisms could conquer multidrug resistance (MDR) of cancer cells and enhance the sensitivity of cancer cells to chemotherapy agents by synergistic effects, thus efficiently supressing tumor progression and reducing side effects [5–10]. Among these combination therapy approaches, the integration of thermal therapy and chemotherapy into a single nanoparticle-based system has received much attention because the tumor-targeted hyperthermia not only causes strong thermal ablation on cancer cells but also enhances the tumor accumulation of drugs by promoting permeability of tumor vessels, thereby significantly improving the efficacy of cancer treatment [5,8,10–14]. Moreover, taking advantage of high tissue penetration, precise spatiotemporal selectivity, minimal invasiveness and phototoxicity of the near-infrared (NIR) irradiation, the NIR-triggered photothermal therapy (PTT) has been widely combined with chemotherapy to amplify the anticancer effects [15–21].

Because of its approval of the United States Food and Drug Administration for clinical use and superior capability of converting NIR light to generate hyperthermia, indocyanine green (ICG), an amphiphilic tricarbocyanine dye, has been extensively utilized as the PTT agent and incorporated with various chemotherapy drugs such as doxorubicin (DOX) [5,15–18], paclitaxel (PTX) [19], or cisplatin [20,21] into a single nanoformulation for chemo-photothermal combination therapy. Zhang and co-workers fabricated the DOX/ICG-encapsulated liposome-coated thermosensitive nanogels by in situ polymerization [15]. The cargo-loaded nanogels showed the NIR-evolved

* Corresponding author.
E-mail address: whchiang@dragon.nchu.edu.tw (W.-H. Chiang).

https://doi.org/10.1016/j.eurpolymj.2018.11.038
Received 9 September 2018; Received in revised form 21 November 2018; Accepted 22 November 2018
Available online 23 November 2018

coincident DOX liberation and hyperthermia, thus efficiently killing 4T1 murine breast cancer cells by chemo-photothermal synergistic effects. Moreover, Cai's group found that the lipid-polymer nanoparticles carrying both DOX and ICG significantly inhibited the progression and recurrence of DOX-sensitive MCF-7 and DOX resistant MCF-7 tumor by the NIR laser-triggered hyperthermia capable of inhibiting the P-glycoprotein (P-gp) mediated drug efflux to increase drug accumulation inside cancer cells [5]. In our previous work [16], the potent imaging-guided photothermal/chemo combinatorial therapy of the surface charge-changeable ICG/DOX-containing nanoparticles accumulated within TRAMP-C1 tumor caused considerable tumor tissue/vessel ablation, thereby further augmenting their extravasation and DOX tumor penetration to profoundly suppress tumor growth. On the other hand, Ding et al. developed the folate-conjugated nanostructured lipid carriers (NLCs) for tumor-targeted co-delivery of ICG and PTX [19]. Through the speeded PTX liberation and promoted intracellular drug transport driven by NIR radiation-triggered hyperthermia, the cytotoxicity of dual drugs-containing NLCs against HepG2 cells was significantly increased. Furthermore, for cancer targeted delivery of cisplatin and ICG, the folate-modified cisplatin/ICG-loaded lipid-polymer hybrid nanoparticles (FCINPs) were attained by using a single-step sonication method [20]. The treatment of FCINPs combined with 808 nm NIR laser irradiation can appreciably induce the apoptosis and necrosis of MCF-7 cells, in comparison with chemo or photothermal treatment alone.

The aforementioned studies using lipid-polymer nanoparticles, liposome-coated thermosensitive nanogels or surface charge-changeable nanoparticles to deliver DOX and ICG showed the improved efficacy of chemo-photothermal treatment. However, the efficient DOX release of these cargo-loaded nanoparticles only triggered by the additional NIR laser radiation. This most likely leads to the incomplete DOX release of payload-containing nanoparticles within cancer cells in the lack of sufficient NIR irradiation, thus diminishing the synergistic effects of chemo-photothermal therapy. In order to address the above issue, it is thus necessary to develop the multifunctional nanocarriers that not only simultaneously carry DOX and ICG, but also exert the intracellular acid-triggered DOX release to enhance chemo-photothermal synergistic effect. To this end, the amphiphilic graft copolymer comprising pH-sensitive poly(γ-glutamic acid) (γ-PGA) as the hydrophilic backbone and biodegradable poly(lactic-co-glycolic acid) (PLGA) as the hydrophobic grafts were synthesized and used as main material to fabricate the polymeric nanoassemblies (PNAs). Through the electrostatically induced co-association of γ-PGA-g-PLGA chains and DOX molecules, the electrostatic DOX/γ-PGA complexes were encapsulated into compact PLGA-rich core, meanwhile the amphiphilic D-α-tocopheryl polyethylene glycol succinate (TPGS), 1,2-distearoyl-sn-glycero-3-phosphoethanolamine-N-[amino(polyethylene glycol)] (DSPE-PEG) and ICG molecules were hydrophobically anchored at the surfaces of PLGA-rich core as shown in Scheme 1. Apart from the size, zeta potential and morphology, the in vitro photo-stability and NIR-triggered hyperthermia capability of DOX/ICG-loaded PNAs were also investigated in detail. In addition, the DOX release performance of payload-containing PNAs in response to external pH change was explored. Furthermore, the in vitro cellular uptake of DOX/ICG-carrying PNAs by HeLa cells and their NIR-triggered chemo-photothermal anticancer effects were also assessed.

2. Experimental section

2.1. Materials

DOX in HCl salt form was obtained from Seedchem (Australia). ICG was purchased from Chem-Impex (USA). PLGA (M.W. = 10 kDa, [LA]:[GA] = 75:25) was acquired from Green Square (Taiwan), γ-PGA (M_n > 100 kDa) was purchased from Vedan (Taiwan). DSPE-PEG5000 was obtained Avanti Polar Lipids (USA). TPGS, N-hydroxysuccinimide (NHS), N,N′-dicyclohexylcarbodiimide (DCC), 4-dimethylaminopyridine (DMAP), 3-(4,5-dimethyl-thiazol-2yl)-2,5-diphenyl tetrazolium bromide (MTT) and p-nitroso-N,N′-dimethylaniline (RNO) were purchased from Sigma-Aldrich (USA). Dulbecco's modified Eagle medium (DMEM), Hoechst 33342, propidium iodide (PI) and fetal bovine serum (FBS) were purchased from Invitrogen. DMSO-d_6 used in ^{1}H NMR measurements was obtained from Cambridge Isotope (MA, USA). Deionized water was produced from Milli-Q Synthesis (18 MΩ, Millipore). All other chemicals were reagent grade and used as received.

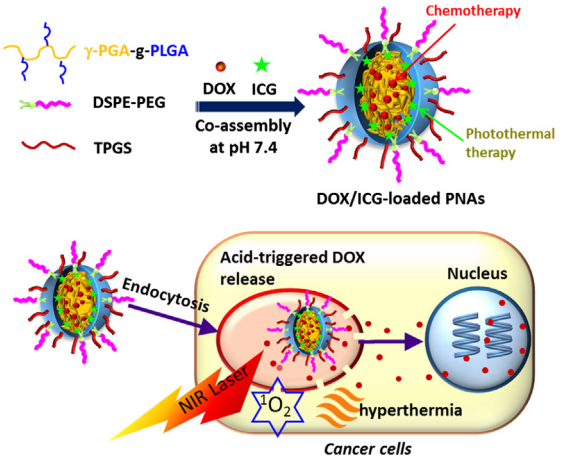

Scheme 1. Schematic illustration of development of DOX/ICG-loaded PNAs for acid-triggered rapid DOX release, and NIR-mediated hyperthermia and singlet oxygen generation.

2.2. Synthesis of γ-PGA-g-PLGA copolymer

The γ-PGA-g-PLGA copolymer utilized in the work was attained by the ester-linkage-based conjugation of the hydroxyl end of PLGA with the reactive glutamyloxysuccinimide (γ-GAOSu) moieties of the poly(γ-GA-co-GAOSu) and then hydrolysis of unreacted γ-GAOSu groups into γ-GA residues as revealed in Scheme 2. γ-PGA (250 mg, 2.1×10^{-3} mol), NHS (120 mg, 1.05×10^{-3} mol), DCC (216 mg, 1.05×10^{-5} mol) and DMAP (128 mg, 1.05×10^{-3} mol) were dissolved in dry DMSO (2.0 mL). The reaction was carried out under stirring at 25 °C for 72 h, followed by the filtration to eliminate dicyclohexylcarbodiurea, the byproduct. Subsequently, the grafting reaction of poly(γ-GA-co-γ-GAOSu) in DMSO with PLGA (20 mol% with respect to NHS residues) was carried out under stirring at 25 °C for 72 h. The solution was then dialyzed (Cellu Sep MWCO 50000) against DMSO for 48 h to remove the unreacted PLGA and reactants. Subsequently, excess pH 7.4 tris buffer was added into the polymer solution to facilitate the hydrolysis of unreacted GAOSu moieties in graft copolymer into γ-GA units, followed by dialysis (Cellu Sep MWCO 6000–8000) against deionized water at 4 °C for 48 h to eliminate DMSO and NHS. The final product was attained by freeze-drying and characterized by ^{1}H NMR, using DMSO-d_6 as the solvent.

2.3. Preparation of cargo-loaded PNAs

The preparation of DOX/ICG-loaded PNAs was performed by the following procedure. γ-PGA-g-PLGA (6.0 mg), DSPE-PEG (0.6 mg), DOX (0.6 mg) and ICG (0.6 mg) were dissolved in DMSO (0.4 mL). The mixture was added dropwise into pH 7.4 phosphate buffer (ionic strength 0.01 M, 3.6 mL) containing TPGS (0.6 mg) under stirring. The solution was mildly stirred in dark at room temperature for 1 h and then equilibrated for 30 min. To remove the unloaded drug and DMSO, DOX/ICG-loaded PNA solution was dialyzed (Cellu Sep MWCO 12,000–14,000) with pH 7.4 phosphate buffer at 4 °C. For comparison,

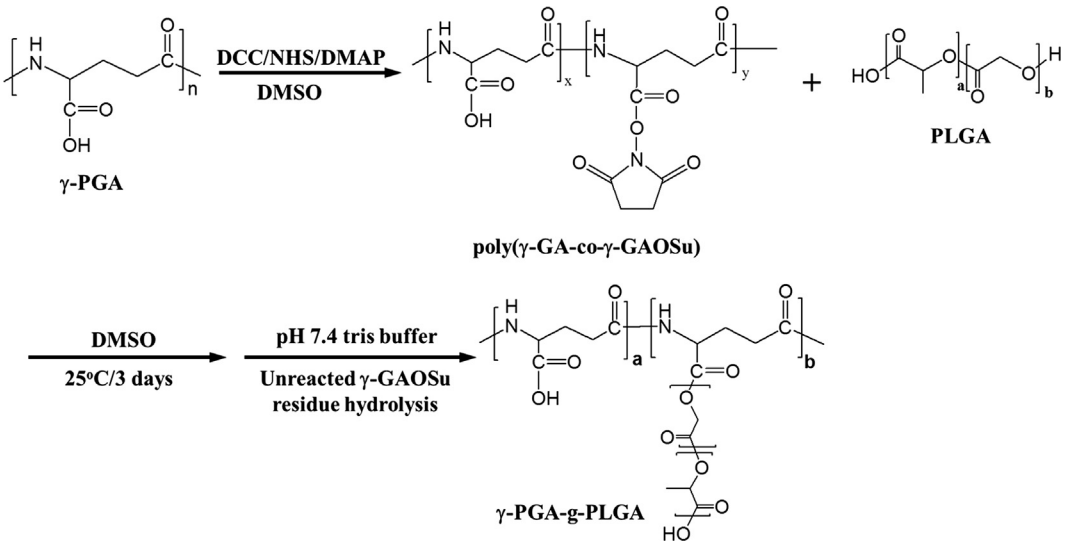

Scheme 2. Synthetic route of γ-PGA-g-PLGA copolymer.

the pristine PNAs and PNAs loaded with either DOX or ICG were also prepared in a similar manner.

2.4. Characterization of pristine PNAs and cargo-loaded PNAs

The hydrodynamic diameter (D_h), size distribution (polydispersity index, PDI) and zeta potential of pristine PNAs and cargo-loaded PNAs in pH 7.4 phosphate buffer were measured by a ZetaSizer Nano Series instrument (Malvern Instruments, U.K.). The data shown here represent an average of at least triplicate measurements. The morphology of pristine PNAs and cargo-loaded PNAs was attained by transmission electron microscopy (TEM) (HT7700, Hitachi, Japan). The UV/Vis absorption spectra of free ICG and ICG-containing PNAs in phosphate buffered saline (PBS) were acquired at different time intervals utilizing a UV/Vis spectrophotometer (U2900, Hitachi, Japan). To examine the loading level of DOX and ICG, a prescribed volume of the purified payload-carrying PNA solution was lyophilized and then dissolved in DMSO to completely disrupt nanoassembly structure for payload release. The DOX fluorescence in the range 500–700 nm was determined by a fluorescence spectrophotometer (F-7000, Hitachi, Japan) while the absorbance of ICG at 775 nm was gained by a UV/Vis spectrophotometer (U2900, Hitachi, Japan). The DOX and ICG calibration curves used for drug loading characterization were presented in Fig. S1. The drug loading efficiency (LE) and loading capacity (LC) were calculated using the following equations:

LE (%) = (weight of loaded drug/weight of drug in feed) × 100%.

LC (%) = (weight of loaded drug/weight of lyophilized drug-loaded PNAs) × 100%.

2.5. Temperature change under NIR laser irradiation

DOX/ICG-containing PNAs and free ICG in PBS (1.0 mL) were irradiated by NIR laser of 808 nm (1.25 W/cm^2) for 10 min. During NIR laser irradiation, the solution temperature was measured by an infrared thermal imaging camera (Thermo Shot F20, NEC Avio Infrared, Germany). The temperature change of DOX/ICG-loaded PNA solutions (ICG concentration = 10 μM) exposed to NIR laser irradiation of different power densities was also monitored.

2.6. In vitro measurement of singlet oxygen ($^1O_2$)

13 mM of RNO and 15 mM of histidine in phosphate buffer (10 mM, pH 7.4) were mixed with the ICG-loaded PNA solution and free ICG solution at a fixed ICG concentration of 10 μM. The mixed solutions were then irradiated with a NIR laser of 808 nm (1.25 W/cm^2) for 5 min. The generation of singlet oxygen by ICG-loaded PNAs or free ICG was explored by determining the variation of characteristic absorbance of RNO at 440 nm using by a UV/Vis spectrophotometer (U2900, Hitachi, Japan).

2.7. In vitro drug release profiles

For DOX release assessment, the dialysis (Cellu Sep MWCO 12,000–14,000) of the DOX/ICG-loaded PNA solutions (1.0 mL) against PBS (pH 7.4) and succinic acid buffer (pH 5.0) (ionic strength 0.15 M, 30 mL), respectively, was conducted at 37 °C. At various time intervals, 1.0 mL of dialysate was withdrawn for analysis and replaced with an equal volume of fresh medium. The amount of released DOX was attained by fluorescent measurement. On the other hand, for ICG liberation test, the DOX/ICG-loaded PNA solution (2.0 mL) and free ICG solution (2.0 mL) as a control were dialyzed (Cellu Sep MWCO 12,000–14,000) with PBS (pH 7.4) (ionic strength 0.15 M, 40 mL), respectively, at 37 °C. The internal sample solution was taken periodically for determination of ICG absorbance at 775 nm. The sample solution was placed back into the dialysis tube after each measurement. The cumulative ICG release (%) was obtained by the formula:

Cumulative ICG release (%) = ((Initial ICG absorbance – ICG absorbance at different time points)/initial ICG absorbance) × 100%. The data presented herein represent an average of triplicate measurements.

2.8. In vitro cellular uptake

Free DOX and DOX/ICG-loaded PNAs were dispersed in DMEM to a DOX concentration of 20 μM. HeLa cells (4×10^6 cells/well) seeded in 12-well culture plates were incubated with the above solutions at 37 °C for 1 and 3 h, respectively. After prescribed incubation, the treated HeLa cells were washed three times with PBS and separated with trypsine-EDTA solution, followed by suspension in PBS (1.0 mL) to attain a cell suspension. The FACSCalibur flow cytometer (BD Bioscience) was exploited to evaluate DOX cellular uptake. A minimum of 1×10^4 cells were analysed from each batch with fluorescence intensity presented on a three-decade log scale. Moreover, based on the above manner, after being washed three times with PBS, the treated HeLa cells in 12-well culture plates were disrupted by addition of DMSO (0.65 mL) for drug extraction. The amount of DOX internalized by HeLa cells was quantitatively determined by fluorescence measurements using a fluorescence spectrophotometer (F-7000, Hitachi, Japan) and the pertinent calibration curve of DOX with various concentrations in DMSO

(Fig. S1), while the fluorescence signals of ICG (745 nm excitation and 810 nm filter) were collected by an in vivo imaging system (IVIS) (Xenogen IVIS Spectrum). On the other hand, HeLa cells (2×10^6 cells/well) were seeded in 6-well plate containing 22 mm round glass coverslips and cultured overnight. Subsequently, the cells were incubated with free DOX, free ICG and DOX/ICG-loaded PNAs at a fixed concentration of 10 μM for DOX and 6.5 μM for ICG at 37 °C for 1 h. After triplicate washing with PBS and fixing with 4% formaldehyde, the cells were stained with Hoechst 33342 for 15 min, and the slides were rinsed three times with PBS. The cellular fluorescence images were attained using a confocal laser scanning microscopy (CLSM) (Zeiss LSM 780, Jena, Germany) at the excitation wavelengths of 355, 488 and 633 nm for Hoechst, DOX and ICG, respectively.

2.9. In vitro cytotoxicity analysis

HeLa cells (2×10^5 cells/well) were seeded in a 24-well plate and incubated at 37 °C for 24 h in DMEM containing 10% FBS and 1% penicillin. The spent medium was then replaced with 1.0 mL of fresh medium containing free DOX, free ICG or various cargo-loaded PNAs and further incubated for additional 6 h. Upon washing twice with PBS, cells were detached by trypsin-EDTA and centrifuged. Afterward, the collected cell pellet colloids were dispersed in DMEM (20 μL) and irradiated by 808 nm laser (1.25 W/cm^2) for 5 min. The laser-treated cells were reseeded in a 96-well plate and incubated for additional 18 h. Then, 200 μL of MTT (0.25 mg/mL) was added into each well and was incubated at 37 °C for additional 4 h. After discarding the culture medium, 0.2 mL DMSO was added into each well to dissolve the precipitate and the resulting solution was measured for absorbance at 570 nm using a FLUOstar OPTIMA microplate reader. The viability of HeLa cells incubated with various payload-carrying PNAs in the absence of NIR laser irradiation was assessed in a similar approach. On the other hand, the cytotoxicity of single photothermal therapy delivered by PNAs against HeLa cells was assessed by Hoechst/PI staining. After being incubated with either free ICG or ICG-loaded PNAs (ICG concentration = 6.5 μM) for 4 h, HeLa cells (2×10^6 cells/well) were irradiated by 808 nm NIR laser (1.25 W/cm^2) for 5 min at a selected region. Finally, the cells were double stained with PI and Hoechst 33342, and then observed on a Nikon ECLIPSE Ti-U inverted microscope.

3. Results and discussion

3.1. Synthesis and characterization of γ-PGA-g-PLGA copolymer

By partial transesterification of poly(γ-GA-co-γ-GAOSu) with PLGA segments and subsequent complete hydrolysis of the residual γ-GAOSu groups into the γ-GA residues, the γ-PGA-g-PLGA copolymer used in this study was obtained. As shown in DOSY ^{1}H NMR spectrum of γ-PGA-g-PLGA in DMSO-d_6 (Fig. S2), the characteristic proton signals from the γ-PGA and PLGA in the graft copolymer are observed at the same diffusion coefficient, confirming the successful conjugation of γ-PGA with PLGA segments. The ^{1}H NMR spectrum of γ-PGA-g-PLGA copolymer in DMSO-d_6 was presented in Fig. 1. According to the signal integral ratio of the characteristic glutamic proton of γ-GA residues at 4.12 ppm and the methyl protons of PLGA at 1.47 ppm, 8.5 mol % of γ-GA units in γ-PGA was conjugated with PLGA segments.

3.2. Preparation and characterization of cargo-loaded PNAs

The DLS results show that the particle size of cargo-loaded PNAs, in particular for the DOX/ICG-loaded PNAs (ca. 109.9 nm in D_h), is much larger than that of the drug-free PNAs (ca. 59.9 nm) (Fig. 2a and Table 1). In addition to the well-dispersed spherical shape, the somewhat enlarged particle size of DOX/ICG-loaded PNAs relative to the pristine PNAs was also observed in the TEM images (Fig. 2b and c), corresponding to the DLS findings. Such a difference in particle size could be attributed to the encapsulation of more drug payloads into hydrophobic core of PNAs, thus enlarging their size [4,22]. Furthermore, it should be mentioned that the particle sizes of DOX/ICG-loaded PNAs and pristine PNAs observed by TEM are smaller than those determined by DLS because of the transition of PNAs from dried state (TEM) to swollen state (DLS) [23,24]. On the other hand, the zeta potentials of PNAs carrying either ICG alone or both DOX/ICG were significantly higher than those of ICG-free PNAs, while the zeta potential of DOX-loaded PNAs was comparable to that of pristine PNAs (Table 1). In view of amphiphilic property of ICG molecules, it was assumed that the ICG species were apt to insert into the DSPE-PEG/TPGS-coated surfaces of PNAs upon cooperative hydrophobic alkyl stacking, thus exposing its two anionic sulfonate groups on colloidal surfaces to increase zeta potential (Scheme 1). By contrast, the DOX molecules were largely entrapped within the solid PLGA-rich core of PNAs by developing hydrophobic electrostatic complexes with the γ-PGA segments [25,26], thus being unable to affect the zeta potential of PNAs. Furthermore, it should be mentioned that the created PNAs loaded with either single drug or dual drugs have adequate drug efficiencies and loading contents (Table 1). Notably, compared to free ICG in PBS, the ICG-containing PNAs exhibited a considerable red shift of the characteristic absorption peak of ICG from 774 nm to 792 nm as presented in Fig. 2d. This reveals that the attachment of ICG molecules to the PNA surface significantly influences their microstructure. Similar findings have also been reported elsewhere [5,16,23].

In order to augment the efficacy of ICG-based cancer photothermal therapy, it is required to enhance photo-stability of ICG in aqueous solution. For assessment of the aqueous photo-stability of ICG, the feature ICG absorbance of ICG-containing PNAs and free ICG (ICG concentration = 10 μM) in PBS (pH 7.4, I = 0.15 M) at 37 °C was monitored over time by UV/Vis spectrophotometer. As shown in Fig. 3a, upon 9-day incubation in PBS, distinct from a considerable reduction in the absorbance of free ICG, the ICG absorbance of ICG-containing PNAs was slightly decreased. Furthermore, based on the UV/Vis spectra obtained at different time points, the feature absorbance of ICG at each time point is normalized to that at the origination as shown in Fig. S3. While the normalized absorbance of free ICG declined markedly after 2 days, only a minor change in absorbance was observed for ICG-carrying PNAs. These results corroborate that the hydrophobic insert of ICG species into DSPE-PEG/TPGS-based surfaces of PNAs can sufficiently suppress self-aggregation and degradation of ICG in aqueous phase, therefore prominently promoting ICG photo-stability. Furthermore, the DOX/ICG-loaded PNAs in PBS at 37 °C maintained unchanged particle size during 4 days similar to drug-free PNAs (Fig. 3b). This suggests that the DSPE-PEG/TPGS-coated surfaces of PNAs could sufficiently prevent inter-particle aggregation by the steric repulsion of hydrophilic PEG segments. On the other hand, the cargo-loaded PNAs stored in phosphate buffer at 4 °C showed an unvaried particle size over a period of 4 weeks (Fig. S4), indicating their superior long-term storage stability.

The hyperthermia ability of the DOX/ICG-loaded PNA solutions during 808 nm laser irradiation (power density of 1.25 W/cm^2) was evaluated by measuring the solution temperature with an infrared thermal imaging camera. Under 2 min NIR laser irradiation, PBS maintained a virtually unchanged temperature, while the DOX/ICG-carrying PNA and free ICG solution (ICG concentration = 10 μM) showed a prominent temperature elevation due to ICG-mediated photothermal conversion effect (Fig. 3c). Moreover, at the same irradiation time, the temperature of DOX/ICG-loaded PNAs solution was somewhat higher than that of free ICG solution because the absorption peak of ICG from the former underwent red-shift (from 774 nm to 792 nm) to approach the central wavelength (808 nm) of the diode laser utilized, thus enhancing the photo-thermal conversion efficiency [16,27]. As expected, the NIR-triggered hyperthermia of DOX/ICG-loaded PNA solution was further promoted with increasing the ICG concentration from

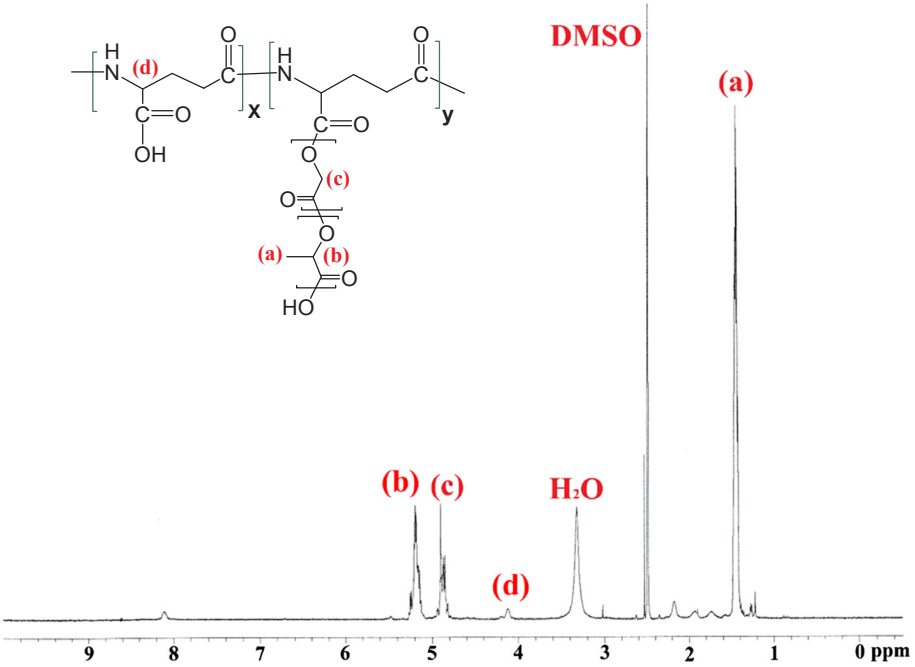

Fig. 1. ^{1}H NMR spectrum of γ-PGA-g-PLGA copolymer in DMSO-d_6.

10 to 30 μM. On the other hand, the temperature of ICG-containing solutions decreased slowly after ca. 3-min NIR laser irradiation. Similar observations have been reported elsewhere [16,23,27]. The decline of photo-triggered hyperthermia effect could be attributed to the photo-bleaching of ICG resulted from a process involving photo-sensitization to form singlet oxygen, dioxetane formation, and then dioxetane cleavage into carbonyl products [28,29]. For ICG/DOX-loaded PNAs exposed to NIR laser irradiation, the photo-bleaching of ICG molecules occurred, being probably because ICG molecules anchored at the PNA surfaces still have access to singlet oxygen generated by photo-sensitization. Furthermore, the photothermal conversion effects of DOX/ICG-loaded PNAs were well regulated by changing laser power density as shown in Fig. 3d.

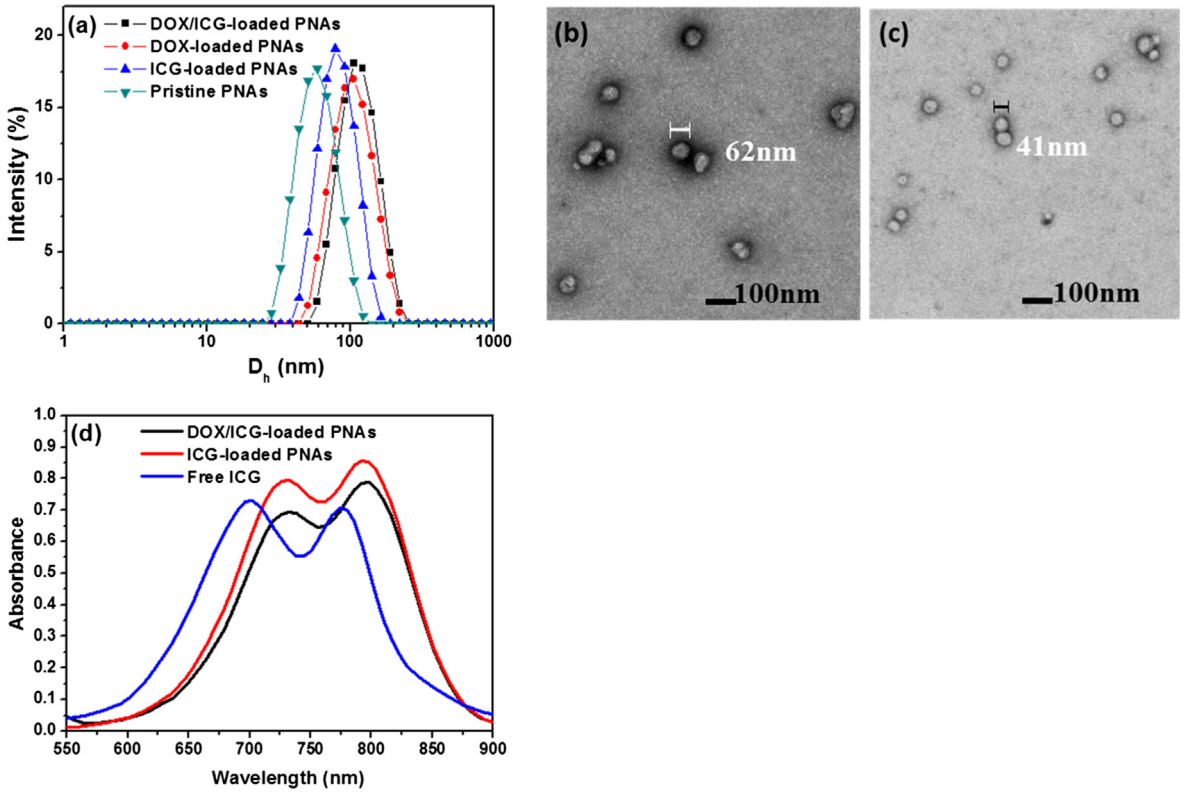

Fig. 2. (a) DLS particle size distribution profiles of pristine PNAs and cargo-loaded PNAs. TEM images of (b) DOX/ICG-loaded PNAs and (c) pristine PNAs. (d) UV/Vis absorption spectra of free ICG, ICG-loaded PNAs, and DOX/ICG-loaded PNAs in PBS.

Table 1
Physicochemical properties, drug loading efficiency and content of cargo-loaded PNAs and pristine PNAs.

Sample	D_h (nm)	PDI	ZP[a] (mV)	DOX LE[b] (%)	DOX LC[c] (wt%)	ICG LE[b] (%)	ICG LC[c] (wt%)
DOX/ICG-loaded PNAs	109.9 ± 1.3	0.08	−28.2 ± 1.3	72.2 ± 2.3	5.5 ± 0.2	70.0 ± 1.5	5.1 ± 0.1
DOX-loaded PNAs	94.7 ± 4.9	0.08	−18.3 ± 1.6	71.3 ± 1.2	5.4 ± 0.1	–	–
ICG-loaded PNAs	85.2 ± 3.0	0.10	−26.9 ± 2.0	–	–	68.6 ± 7.7	5.2 ± 0.6
Pristine PNAs	59.9 ± 3.6	0.11	−15.0 ± 1.1	–	–	–	–

[a] ZP: Zeta potential.
[b] LE: Loading efficiency.
[c] LC: Loading content.

3.3. In vitro singlet oxygen generation

Under NIR laser irradiation, in addition to the hyperthermia capability, ICG also can generate reactive oxygen species (ROS), such as singlet oxygen and superoxide [30]. To confirm the singlet oxygen generation of ICG-carrying PNAs exposed to laser irradiation, the RNO assay was used in this work. As shown in Fig. 4, after NIR laser irradiation, the feature absorbance at 440 nm of RNO in free ICG and ICG-loaded PNA dispersions was appreciably reduced. This strongly proves that the generation of singlet oxygen from free ICG and ICG-loaded PNAs during NIR laser radiation leads to a reaction with imidazole-containing histidine to form a peroxide intermediate, which then oxidizes RNO to cause bleaching of RNO absorbance [31,32].

3.4. In vitro DOX and ICG release study

In view of the encapsulated electrostatic complexes comprising both DOX molecules and pH-responsive γ-PGA segments, they are expected capable of controlling DOX release in response to external pH change. As shown in Fig. 5a, different from a quite fast outflow of free DOX across the dialysis tube in pH 7.4 PBS (> 80% over 3 h), the DOX liberation from payload-containing PNAs under the same condition was significantly reduced. This indicates that the electrostatic DOX/γ-PGA complexes encapsulated within compact PLGA-rich core can efficiently prevent DOX leakage from PNAs at pH 7.4. Notably, with the medium pH being lowered from pH 7.4 to 5.0, the cumulative DOX release of cargo-loaded PNAs was significantly increased (> 70% over 5 h). Such an acid-activated rapid DOX release is attributed to the extensive disruption of ionic DOX/γ-GA pairings upon the decreased ionization degree of γ-GA residues in weak acid milieu [25,26] where the core-

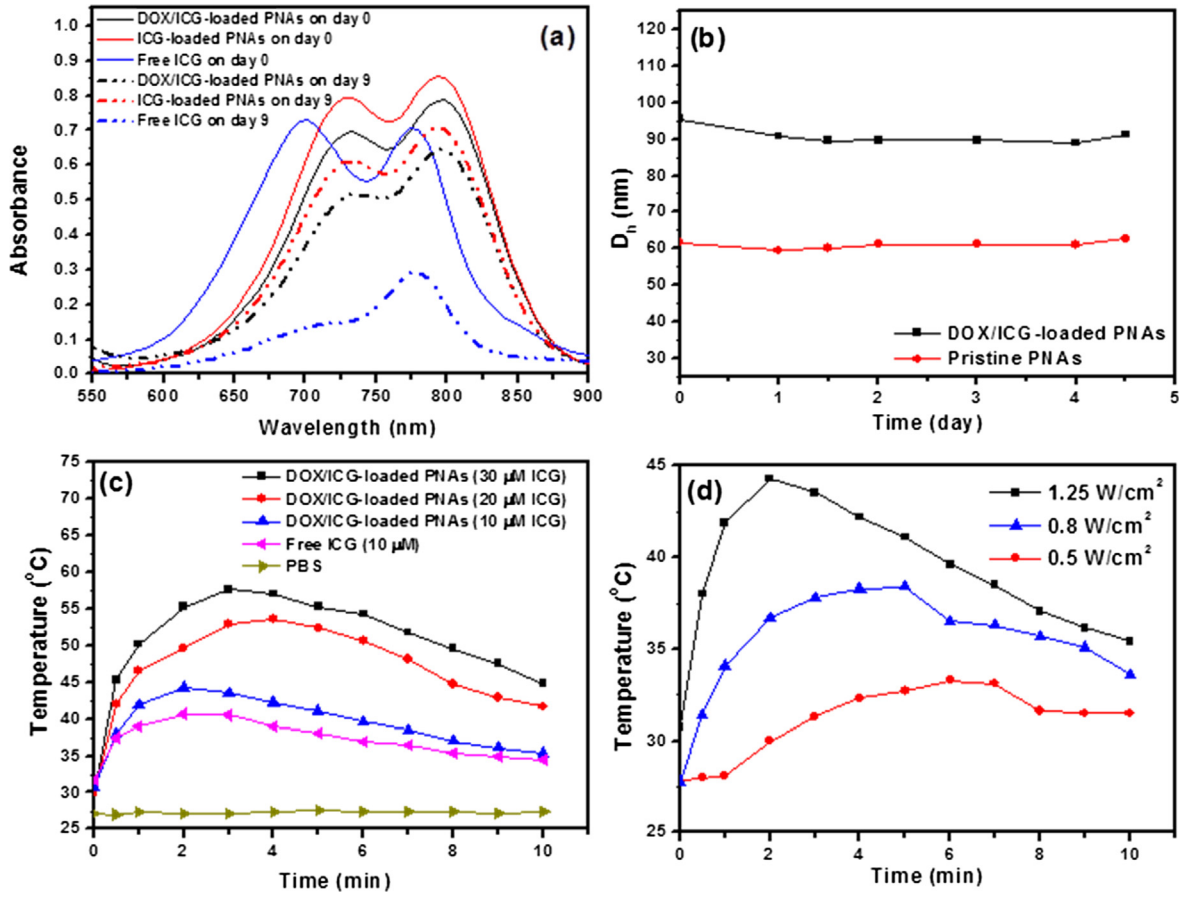

Fig. 3. (a) UV/Vis spectra of free ICG and ICG-containing PNAs suspended in PBS at 37 °C at different time points. (b) Particle size of pristine PNAs and DOX/ICG-loaded PNAs in PBS at 37 °C as a function of time. (c) Temperature profiles of PBS, free ICG and DOX/ICG-loaded PNAs as a function of the irradiation time under 808 nm laser irradiation at a power intensity of 1.25 W/cm^2. (d) Temperature profiles of DOX/ICG-loaded PNAs in PBS with 808 nm NIR laser irradiation of different power densities.

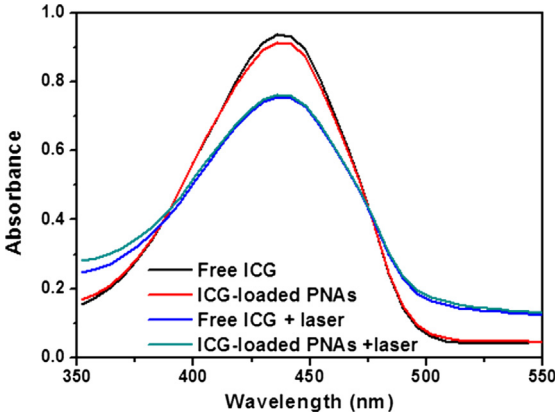

Fig. 4. UV spectra of RNO in free ICG and ICG-loaded PNA dispersions before and after 5-min NIR laser irradiation.

forming PLGA segments are apt to be degraded, thus assisting DOX efflux. On the other hand, an appreciably reduced ICG outflow of cargo-loaded PNAs relative to that of free ICG was observed in pH 7.4 PBS (Fig. 5b). This reveals that the hydrophobic insert of amphiphilic ICG molecules into the DSPE-PEG/TPGS-covered surfaces of PNAs could reduce the undesired ICG leakage. It should be mentioned that for DOX/ICG-loaded PNAs at pH 7.4, a continued ICG release occurred throughout the test whereas the DOX release reached a plateau after 5 h, implying the distinct distribution of DOX and ICG payloads in cargo-loaded PNAs. DOX species were mostly localized in the interior of PNAs, thus slowing their efflux rate, while the amphiphilic ICG molecules were primarily attached on the PNA surfaces, thereby inevitably proceeding the passive diffusion. Based on the results of zeta potential (Table 1) and in vitro drug release (Fig. 5), the attained DOX/ICG-loaded PNAs featured a compact γ-PGA/DOX complexes-encapsulated PLGA-rich core coated with the co-assembly of TPGS, DSPE-PEG and ICG molecules (Scheme 1), and exhibited the reduced ICG premature leakage and acid-triggered DOX release, thus showing great promise to promote intracellular delivery of chemo-photothermal therapy. Despite the hydrophobic insert of amphiphilic ICG molecules into the DSPE-PEG/TPGS-covered surfaces of PNAs partly reduced ICG leakage, over 60% leakage of ICG within 24 h could lead to the insufficient accumulation of ICG in tumor region, thereby diminishing the antitumor efficacy of PTT. In order to further decrease ICG leakage from nanovehicles, our next work is to achieve efficient encapsulation of ICG molecules into the hydrophobic core of PNAs instead of the amphiphilic surfaces.

3.5. In vitro cellular uptake

In order to confirm intracellular co-delivery of DOX and ICG by PNAs, the cellular internalization of DOX/ICG-loaded PNAs by HeLa cells was evaluated by flow cytometry, IVIS and CLSM. As presented in the flow cytometric histograms of Fig. 6a, compared to HeLa cells without any drug treatment used as a negative control, HeLa cells incubated with either free DOX or DOX/ICG-loaded PNAs (DOX concentration = 20 μM) exhibited considerably enhanced DOX fluorescence intensity as the incubation time was prolonged from 1 h to 3 h, suggesting the increased cellular uptake of DOX and DOX/ICG-loaded PNAs. Interestingly, at the same incubation time, the DOX fluorescence intensity of HeLa cells treated with DOX/ICG-loaded PNAs was higher than that of cells exposed to free DOX. Also, after 3 h incubation, the amount of intracellular DOX of HeLa cells treated with DOX/ICG-loaded PNAs quantified by fluorescence measurements using a fluorescence spectrophotometer was ca. 1.4-fold enhanced compared to that of cells incubated with free DOX (Fig. 6b). On the other hand, after 3 h incubation, the fluorescence signals of ICG molecules from HeLa cells incubated with DOX/ICG-containing PNAs were 1.3-fold higher than that from cells incubated with free ICG (Fig. 6c). These findings suggest that the created DOX/ICG-loaded PNAs can effectively boost the intracellular delivery of DOX and ICG molecules. Such an enhanced intracellular cargo transport is resulted probably from the inhibition of the P-glycoprotein mediated drug efflux by TPGS molecules detached from the surfaces of endocytosed PNAs. Similar phenomenon based on TPGS-containing nanocarriers was also mentioned elsewhere [33,34].

As shown in the CLSM images (Fig. 7), a significant DOX fluorescence was observed in the nucleus region of HeLa cells incubated with DOX/ICG-loaded PNAs for 1 h, being comparable to that of cells treated with free DOX. This demonstrates that the endocytosed DOX/ICG-loaded PNAs within acidic endosomes and lysosomes can rapidly release DOX molecules, thus facilitating translocation of DOX from cytoplasm to cell nucleus. On the other hand, ICG fluorescence was largely found in the cytoplasm of HeLa cells exposed to either DOX/ICG-loaded PNAs or free ICG, which being parallel to the previous studies that ICG molecules were mostly bound to intracellular protein (glutathione S-transferase) [5,35]. Based on the above results, evidently, DOX and ICG molecules could be efficiently delivered to the same cancer cells by the cargo-loaded PNAs.

3.6. In vitro chemo-photothermal therapy

To assess the therapeutic efficacy of DOX chemotherapy combined with ICG-based NIR-triggered photothermal therapy, the viability of HeLa cells incubated with PNAs carrying either single- or dual-modality

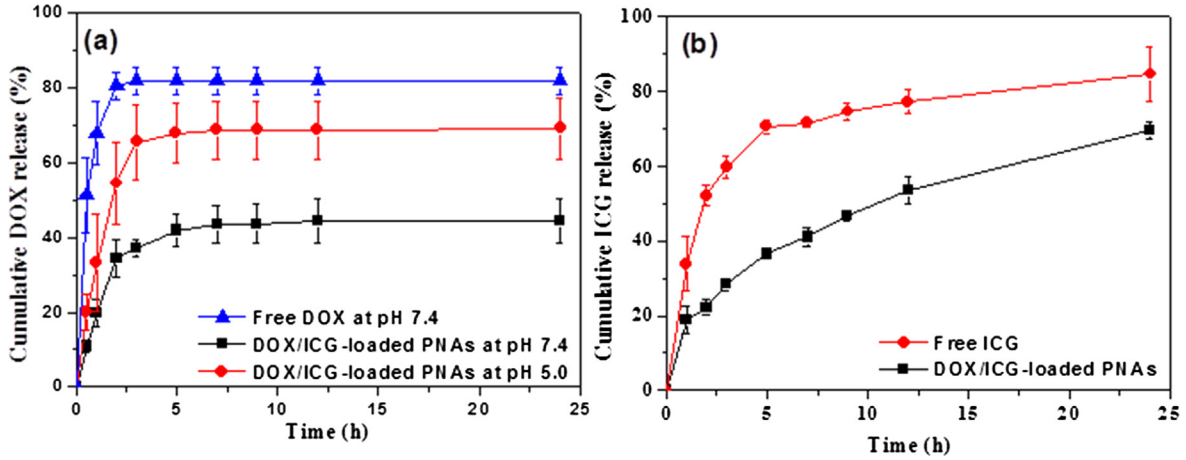

Fig. 5. (a) Cumulative DOX release profiles of DOX/ICG-loaded PNAs in aqueous solutions of pH 5.0 and 7.4 at 37 °C. (b) Cumulative ICG release profile of DOX/ICG-loaded PNAs in PBS at 37 °C. For comparison, diffusion of free DOX and ICG across the dialysis tube in PBS is included.

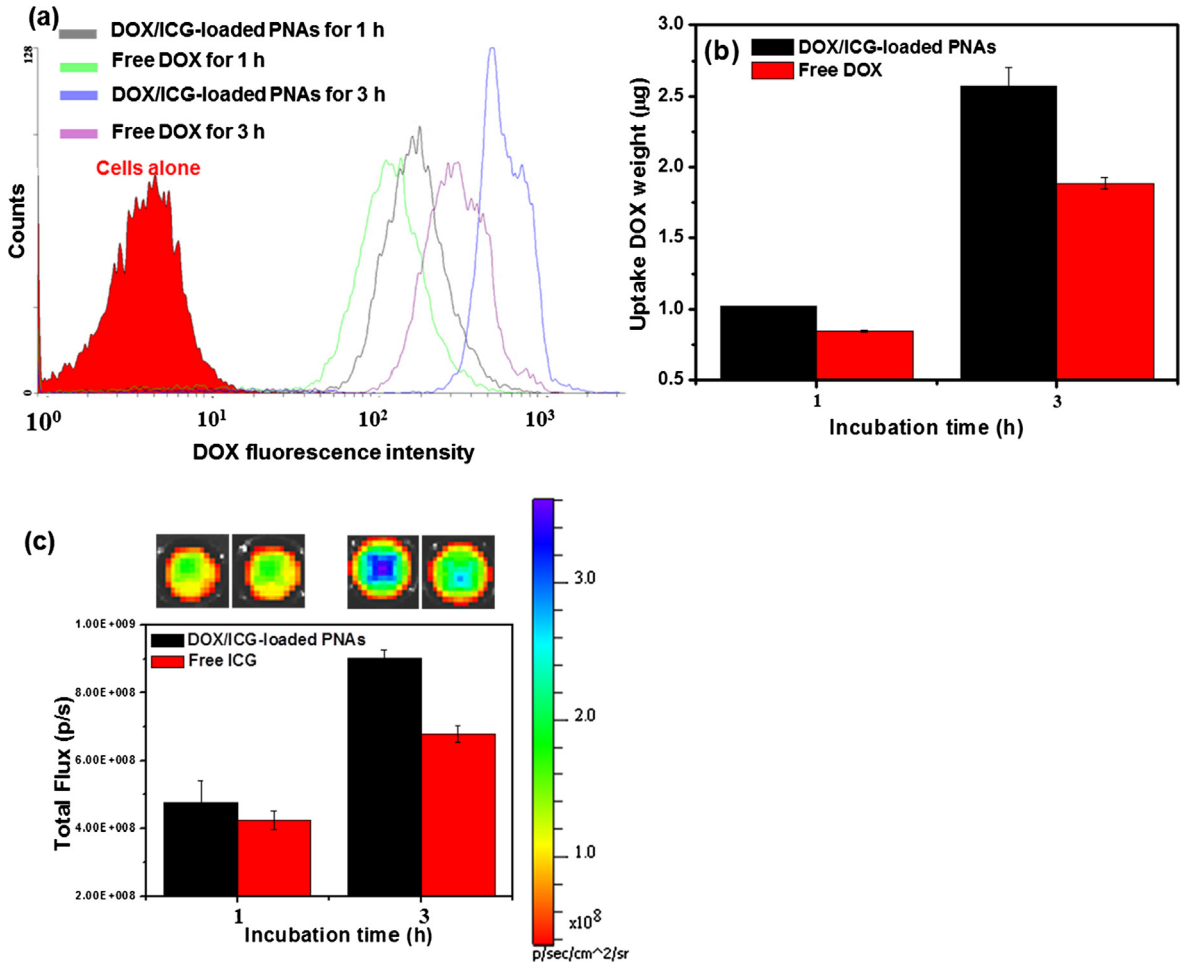

Fig. 6. (a) Flow cytometric histogram and (b) intracellular DOX amount of HeLa cells incubated with free DOX and DOX/ICG-loaded PNAs (DOX concentration = 20 μM) at 37 °C for 1 and 3 h, respectively. (c) NIR fluorescence images and intensity of ICG molecules from HeLa cells treated with free ICG and DOX/ICG-loaded PNAs (ICG concentration = 13 μM) at 37 °C for 1 and 3 h, respectively.

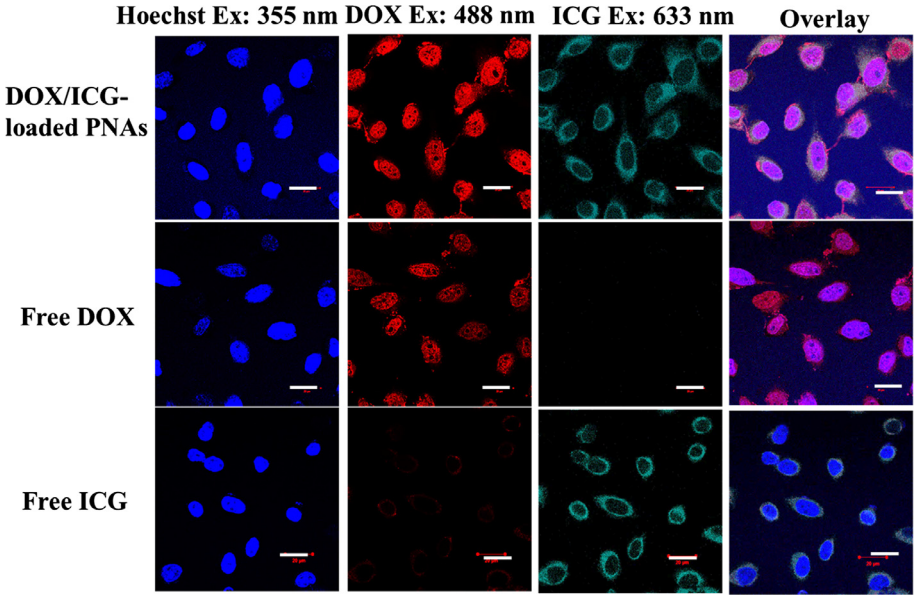

Fig. 7. (a) CLSM images of HeLa cells treated with free DOX, free ICG or DOX/ICG-loaded PNAs at 37 °C for 1 h. Cell nuclei were stained with Hoechst 33342. Scale bars are 20 μm.

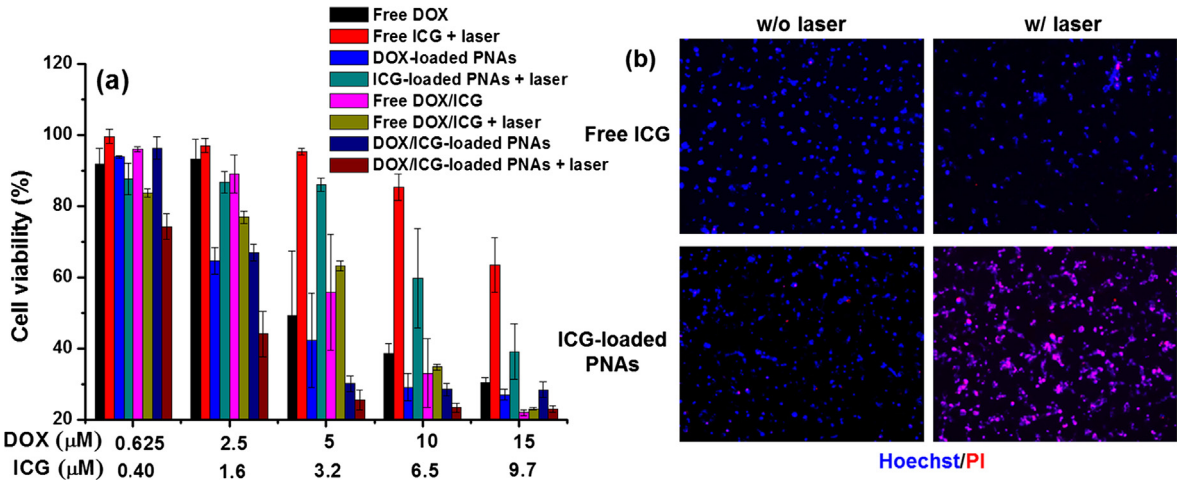

Fig. 8. (a) Cell viability of HeLa cells incubated with various formulations for 6 h with and without 5-min NIR laser irradiation, followed by additional 18-h incubation. (b) Fluorescence images of HeLa cells treated with free ICG or ICG-loaded PNAs with and without laser irradiation. An ICG concentration of 6.5 μM was used. Viable cells are Hoechst 33342-positive and PI-negative, whereas dead cells are Hoechst 33342-positive and PI-positive.

therapy was examined by MTT assay. In comparison with a relatively high viability (beyond 95%) of HeLa cells incubated with either free ICG or ICG-loaded PNAs at an ICG concentration of 9.7 μM in the absence of NIR radiation (Fig. S5), the viability of the treated HeLa cells was appreciably reduced upon 5 min NIR laser radiation, indicating that the NIR-triggered hyperthermia induced cell death (Fig. 8a). Notably, the ICG-loaded PNAs exhibited a prominent photo-triggered cytotoxicity relative to free ICG. Furthermore, at an ICG concentration of 6.5 μM with NIR laser irradiation, such low PI signals of HeLa cells incubated with free ICG is indicative of few cell death (Fig. 8b), corresponding to the high viability (ca. 85%) of ICG-treated HeLa cells (Fig. 8a). By contrast, at the same ICG concentration, most of HeLa cells treated with ICG-loaded PNAs and NIR laser irradiation presented obvious PI-positive staining, signifying extensive cell death (Fig. 8b). The results are primarily attributed to that the ICG-loaded PNAs can significantly enhance the aqueous photo-stability and intracellular delivery of ICG, thus showing the NIR-triggered powerful thermal ablation on HeLa cells. On the other hand, at a DOX concentration of 10 and 15 μM without NIR laser irradiation, the viability of HeLa cells incubated with PNAs carrying either DOX alone or both DOX/ICG was comparable to that of HeLa cells treated with free DOX alone or free DOX/ICG. This indicates that the pH-triggered rapid DOX liberation from cargo-loaded PNAs within acidic organelles could facilitate the deposition of DOX within nucleus, thereby maximizing the therapeutic efficiency of chemotherapy. Furthermore, at high drug concentrations, no significant reduction in the viability of HeLa cells treated with either free DOX/ICG or DOX/ICG-loaded PNAs was observed upon the additional NIR laser irradiation. Obviously, at high drug dosage, the DOX-based chemotherapy plays a predominant role in the anticancer effect relative to the photothermal therapy mediated by ICG.

Notably, when the DOX and ICG doses were decreased to 2.5 μM and 1.6 μM, respectively, the cytotoxicity of DOX/ICG-carrying PNAs against HeLa cells was further boosted by the extra NIR laser irradiation. Moreover, at the same ICG concentration, only a slight reduction in the viability of HeLa cells treated with ICG-loaded PNAs and laser irradiation was observed. According to the above results, at low drug doses, the single chemotherapy or photothermal therapy cannot efficiently kill HeLa cells, whereas the chemo-photothermal combination therapy of DOX/ICG-loaded PNAs effectively inhibits proliferation of cancer cells. It was assumed that the endocytosed DOX/ICG-loaded PNAs under NIR laser irradiation probably disrupted endosomal membranes by ICG-mediated hyperthermia as well as singlet oxygen generation [36,37], thus making DOX molecules escape from endosomes and translocate into nuclei region to augment the cytotoxicity (Scheme 1). Also, the strategy of promoting endosomal escape of chemotherapy drugs by the NIR-triggered mild hyperthermia or singlet oxygen generation of various photosensitizers has been widely adopted [38,39].

4. Conclusions

To improve the outcome of the chemo-photothermal cancer therapy, the γ-PGA-g-PLGA-based PNAs were developed to serve as a vehicle of DOX and ICG molecules. The DOX/ICG-loaded PNAs were characterized by the electrostatic DOX/γ-PGA complexes-encapsulated PLGA-rich core stabilized by the ICG-containing DSPE-PEG/TPGS-constituted surfaces. The DOX/ICG-carrying PNAs not only significantly promoted the photo-stability of ICG in PBS, but also reduced ICG burst leakage. Moreover, by massive disruption of ionic DOX/γ-GA parings and PLGA degradation under weak acidic condition, the DOX release of cargo-loaded PNAs was considerably accelerated. In vitro cellular uptake study indicates that the DOX/ICG-loaded PNAs can enhance cellular uptake of cargoes by HeLa cells. Importantly, taking advantage of the acid-triggered rapid DOX release combined with the photo-induced hyperthermia and singlet oxygen generation to facilitate accumulation of DOX within nucleus, even at low drug dosage, the DOX/ICG-loaded PNAs effectively suppressed the proliferation of cancer cells. Based on these findings, the DOX/ICG-loaded PNAs display the great potential for augmenting efficacy of the chemo-photothermal cancer therapy.

Acknowledgements

This work is supported by the Ministry of Science and Technology (NSC 102-2218-E-007-007 and MOST 103-2221-E-007-023), Taiwan.

Appendix A. Supplementary material

Supplementary data to this article can be found online at https://doi.org/10.1016/j.eurpolymj.2018.11.038.

References

[1] J. Shi, P.W. Kantoff, R. Wooster, O.C. Farokhzad, Cancer nanomedicine: progress, challenges and opportunities, Nat. Rev. Cancer 17 (2017) 20–37.
[2] T. Weia, C. Chen, J. Liu, C. Liu, P. Posocco, X. Liu, Q. Cheng, S. Huo, Z. Liang, M. Fermeglia, S. Pricl, X.J. Liang, P. Rocchi, L. Peng, Anticancer drug nanomicelles formed by self-assembling amphiphilic dendrimer to combat cancer drug resistance, PNAS 112 (2015) 2978–2983.
[3] J.P. Quinones, J. Jokinen, S. Keinänen, C.P. Covas, O. Brüggemann, D. Ossipov, Self-assembled hyaluronic acid-testosterone nanocarriers for delivery of anticancer

drugs, Eur. Polym. J. 99 (2018) 384–393.
[4] X. Zhu, A. Tsend-Ayush, Z. Yuan, J. Wen, J. Cai, S. Luo, J. Yao, J. Bian, L. Yin, J. Zhou, J. Yao, Glycyrrhetinic acid-modified TPGS polymeric micelles for hepatocellular carcinoma-targeted therapy, Int. J. Pharm. 529 (2017) 451–464.
[5] M. Zheng, C. Yue, Y. Ma, P. Gong, P. Zhao, C. Zheng, Z. Sheng, P. Zhang, Z. Wang, L. Cai, Single-step assembly of DOX/ICG loaded lipid–polymer nanoparticles for highly effective chemo-photothermal combination therapy, ACS Nano 7 (2013) 2056–2067.
[6] C. Gao, X. Liang, S. Mo, N. Zhang, D. Sun, Z. Dai, Near-infrared cyanine-loaded liposome-like nanocapsules of camptothecin-floxuridine conjugate for enhanced chemophotothermal combination cancer therapy, ACS Appl. Mater. Interfaces 10 (2018) 3219–3228.
[7] X. Pang, J. Wang, X. Tan, F. Guo, M. Lei, M. Ma, M. Yu, F. Tan, N. Li, Dual-modal imaging-guided theranostic nanocarriers based on indocyanine green and mTOR inhibitor rapamycin, ACS Appl. Mater. Interfaces 8 (2016) 13819–13829.
[8] J.H. Fang, Y.T. Lee, W.H. Chiang, S.H. Hu, Magnetoresponsive virus-mimetic nanocapsules with dual heat-triggered sequential-infected multiple drug-delivery approach for combinatorial tumor therapy, Small 11 (2015) 2417–2428.
[9] H. Wang, J. Wu, K. Xie, T. Fang, C. Chen, H. Xie, L. Zhou, S. Zheng, Precise engineering of prodrug cocktails into single polymeric nanoparticles for combination cancer therapy: extended and sequentially controllable drug release, ACS Appl. Mater. Interfaces 9 (2017) 10567–10576.
[10] C.M. Hu, S. Aryal, L. Zhang, Nanoparticle-assisted combination therapies for effective cancer treatment, Therap. Deliv. 1 (2010) 323–334.
[11] H. Gao, Y. Bi, X. Wang, M. Wang, M. Zhou, H. Lu, J. Gao, J. Chen, Y. Hu, Near-infrared guided thermal-responsive nanomedicine against orthotopic superficial bladder cancer, ACS Biomater. Sci. Eng. 3 (2017) 3628–3634.
[12] T. Zheng, G.G. Li, F. Zhou, R. Wu, J.J. Zhu, H. Wang, Gold-nanosponge-based multistimuli-responsive drug vehicles for targeted chemo-photothermal therapy, Adv. Mater. 28 (2016) 8218–8226.
[13] Z. Deng, Y. Xiao, M. Pan, F. Li, W. Duan, L. Meng, X. Liu, F. Yan, H. Zheng, Hyperthermia-triggered drug delivery from iRGDmodified temperature-sensitive liposomes enhances the anti-tumor efficacy using high intensity focused ultrasound, J. Controlled Release 243 (2016) 333–341.
[14] Sato, M. Umemura, K. Mitsudo, H. Fukumura, J.H. Kim, Y. Hoshino, H. Nakashima, M. Kioi, R. Nakakaji, M. Sato, T. Fujita, U. Yokoyama, S. Okumura, H. Oshiro, H. Eguchi, I. Tohnai, Y. Ishikawa, Simultaneous hyperthermia-chemotherapy with controlled drug delivery using single-drug nanoparticles, Sci. Rep. 6 (2016) 24629.
[15] L. Yu, A. Dong, R. Guo, M. Yang, L. Deng, J. Zhang, DOX/ICG coencapsulated liposome-coated thermosensitive nanogels for NIR-triggered simultaneous drug release and photothermal effect, ACS Biomater. Sci. Eng. (2018), https://doi.org/10.1021/acsbiomaterials.8b00379.
[16] C.C. Hung, W.C. Huang, Y.W. Lin, T.W. Yu, H.H. Chen, S.C. Lin, W.H. Chiang, H.C. Chiu, Active tumor permeation and uptake of surface charge-switchable theranostic nanoparticles for imaging-guided photothermal/chemo combinatorial therapy, Theranostics 6 (2016) 302–317.
[17] A. Li, Y. Wang, T. Chen, W. Zhao, A. Zhang, S. Feng, J. Liu, NIR-Laser switched ICG/DOX loaded thermo-responsive polymeric capsule for chemo-photothermal targeted therapy, Eur. Polym. J. 9 (2017) 51–60.
[18] R. Manchanda, A. Fernandez-Fernandez, A. Nagesetti, A. McGoron, Preparation and characterization of a polymeric (PLGA) nanoparticulate drug delivery system with simultaneous incorporation of chemotherapeutic and thermo-optical agents, J. Colloids Surf. B Biointerfaces 1 (2010) 260–267.
[19] X. Ding, X. Xu, Y. Zhao, L. Zhang, Y. Yu, F. Huang, D. Yin, H. Huang, Tumor targeted nanostructured lipid carrier codelivering paclitaxel and indocyanine green for laser triggered synergetic therapy of cancer, RSC Adv. 7 (2017) 35086–35095.
[20] L. Gu, T. Shi, Y. Sun, C. You, S. Wang, G. Wen, L. Chen, X. Zhang, J. Zhu, B. Sun, Folate-modified, indocyanine green-loaded lipid-polymer hybrid nanoparticles for targeted delivery of cisplatin, J. Biomater. Sci. Polym. Ed. 28 (2017) 690–702.
[21] C. You, M. Wang, H. Wu, P. An, M. Pan, Y. Luo, B. Sun, Near infrared radiated stimulus-responsive liposomes based on photothermal conversion as drug carriers for co-delivery of CJM126 and cisplatin, Mater. Sci. Eng. C 80 (2017) 362–370.
[22] X. Wang, H. Tang, C. Wang, J. Zhang, W. Wu, X. Jiang, Phenylboronic acid-mediated tumor targeting of chitosan nanoparticles, Theranostics 6 (2016) 1378–1392.
[23] W.H. Jian, T.W. Yu, C.J. Chen, W.C. Huang, H.C. Chiu, W.H. Chiang, Indocyanine green-encapsulated hybrid polymeric nano-micelles for photothermal cancer therapy, Langmuir 31 (2015) 6202–6210.
[24] C. Zhang, D. Pan, K. Luo, N. Li, C. Guo, X. Zheng, Z. Gu, Dendrimer-doxorubicin conjugate as enzyme-sensitive and polymeric nanoscale drug delivery vehicle for ovarian cancer therapy, Polym. Chem. 5 (2014) 5227–5235.
[25] W.H. Chiang, W.C. Huang, M.Y. Shen, C.H. Wang, Y.F. Huang, S.C. Lin, C.S. Chern, H.C. Chiu, Dual-layered nanogel-coated hollow lipid/polypeptide conjugate assemblies for potential pH-triggered intracellular drug release, PLOS ONE 9 (2014) e92268.
[26] M. Li, W. Song, Z. Tang, S. Lv, L. Lin, H. Sun, Q. Li, Y. Yang, H. Hong, X. Chen, Nanoscaled poly(L-glutamic acid)/doxorubicin-amphiphile complex as pH-responsive drug delivery system for effective treatment of nonsmall cell lung cancer, ACS Appl. Mater. Interfaces 5 (2013) 1781–1792.
[27] X. Zheng, F. Zhou, B. Wu, W.R. Chen, D. Xing, Enhanced tumor treatment using biofunctional indocyanine green-containing nanostructure by intratumoral or intravenous injection, Mol. Pharm. 9 (2012) 514–522.
[28] R. Liu, J. Tang, Y. Xu, Y. Zhou, Z. Dai, Nano-sized indocyanine green j-aggregate as a one-component theranostic agent, Nanotheranostics 1 (2017) 430–439.
[29] A.P. Gorka, R.R. Nani, M.J. Schnermann, Cyanine polyene reactivity: scope and biomedical applications, Org. Biomol. Chem. 13 (2015) 7584–7598.
[30] W.S. Kuo, Y.T. Chang, K.C. Cho, K.C. Chiu, C.H. Lien, C.S. Yeh, S.J. Chen, Gold nanomaterials conjugated with indocyanine green for dual-modality photodynamic and photothermal therapy, Biomaterials 33 (2012) 3270–3278.
[31] D.J. Park, K.H. Min, H.J. Lee, K. Kim, I.C. Kwon, S.Y. Jeong, S.C. Lee, Photosensitizer-loaded bubble-generating mineralized nanoparticles for ultrasound imaging and photodynamic therapy, J. Mater. Chem. B 4 (2016) 1219–1227.
[32] I. Kraljić, S.E. Mohsni, A new method for the detection of singlet oxygen in aqueous solutions, Photochem. Photobiol. 28 (1978) 577–581.
[33] E.M. Collnot, C. Baldes, U.F. Schaefer, K.J. Edgar, M.F. Wempe, C.M. Lehr, Vitamin E TPGS p-glycoprotein inhibition mechanism: influence on conformational flexibility, intracellular ATP levels, and role of time and site of access, Mol. Pharm. 7 (2010) 642–651.
[34] Y. Guo, J. Luo, S. Tan, B.O. Otieno, Z. Zhang, The applications of vitamin E TPGS in drug delivery, Eur. J. Pharm. Sci. 49 (2013) 175–186.
[35] Y. Tang, T. Lei, R. Manchanda, A. Nagesetti, A. Fernandez, S. Srinivasan, A. McGoron, Simultaneous delivery of chemotherapeutic and thermal-optical agents to cancer cells by a polymeric (PLGA) nanocarrier: an in vitro study, Pharm. Res. 27 (2010) 2242–2253.
[36] C. Shirata, J. Kaneko, Y. Inagaki, T. Kokudo, M. Sato, S. Kiritani, N. Akamatsu, J. Arita, Y. Sakamoto, K. Hasegawa, N. Kokudo, Near-infrared photothermal/photodynamic therapy with indocyanine green induces apoptosis of hepatocellular carcinoma cells through oxidative stress, Sci. Rep. 7 (2017) 13958–13966.
[37] X.H. Wang, H.S. Peng, W. Yang, Z.D. Ren, X.M. Liu, Y.A. Liu, Indocyanine green-platinum porphyrins integrated conjugated polymer hybrid nanoparticles for near-infrared-triggered photothermal and two-photon photodynamic therapy, J. Mater. Chem. B 5 (2017) 1856–1862.
[38] J. Tian, L. Xu, Y. Xue, X. Jiang, W. Zhang, Enhancing photochemical internalization of DOX through a porphyrin-based amphiphilic block copolymer, Biomacromolecules 18 (2017) 3992–4001.
[39] C.S. Lee, K. Na, Photochemically triggered cytosolic drug delivery using pH-responsive hyaluronic acid nanoparticles for light-induced cancer therapy, Biomacromolecules 15 (2014) 4228–4238.